

Boundary-induced violation of the Dirac fermion parity and its signatures in local and global tunneling spectra of graphene

Grigory Tkachov and Martina Hentschel

Max Planck Institute for the Physics of Complex Systems, Dresden, Germany

Extended defects in graphene, such as linear edges, break the translational invariance and can also have an impact on the symmetries specific to massless Dirac-like quasiparticles in this material. The paper examines the consequences of a broken Dirac fermion parity in the framework of the effective boundary conditions varying from the Berry-Mondragon mass confinement to a zigzag edge. The parity breaking reflects the structural sublattice asymmetry of zigzag-type edges and is closely related to the previously predicted time-reversal symmetric edge states. We calculate the local and global densities of the edge states and show that they carry a specific polarization, resembling, to some extent, that of spin-polarized materials. The lack of the parity leads to a nonanalytical particle-hole asymmetry in the edge-state properties. We use our findings to interpret recently observed tunneling spectra in zigzag-terminated graphene. We also propose a graphene-based tunneling device where the particle-hole asymmetric edge states result in a strongly nonlinear conductance-voltage characteristics, which could be used to manipulate the tunneling transport.

PACS numbers: 73.20.At,73.22.Gk,73.63.Bd

I. INTRODUCTION

In condensed matter systems with nodal fermionic spectra, quantum description of low-energy excitations can resemble that of the ultrarelativistic electron. The crystal space group imposes a generic restriction on such quasiparticles known as fermion doubling: they come in pairs of opposite chirality species that can be mapped to the conventional "right-handed" (RH) and "left-handed" (LH) fermions of the Dirac theory.¹ The most recently studied examples are graphene, where two distinct Fermi points in the Brillouin zone give rise to both chiral species,^{2,3} and 2D HgTe quantum wells where spin-orbit coupling effectively results in a pair of the RH and LH fermions at low energies.^{4,5,6} The fermion doubling brings the symmetry with respect to the exchange of the chiralities, $\text{RH} \rightleftharpoons \text{LH}$, related to the parity symmetry of the Dirac equation.⁷ It is of considerable interest to investigate the consequences of the violation of such a symmetry, since they could be observable in materials where quasiparticles imitate Dirac electrons. Besides, the Dirac fermion parity is distinct from other discrete symmetries (e.g. time-reversal invariance), and, therefore, through its violation one could achieve additional control over electronic properties of the material.

It has been noticed^{8,9} that discrete symmetries of a Dirac fermion system can be broken, along with the translational invariance, by the boundaries of the system. In this paper we focus on the parity violation due to such a boundary effect and suggest how to detect and, possibly, use it in electronic devices.

Our main assumption is that the boundary does not cause scattering between the opposite chirality quasiparticles. To model this we use effective boundary conditions,^{8,9} interpolating between the infinite mass confinement¹⁰ and the zigzag graphene boundary.^{11,12} The parity breaking occurs as long as the boundary devi-

ates from the infinite mass confinement toward the zigzag edge. This is due to the structural sublattice asymmetry: a zigzag-type crystal face has unequal numbers of sites from the two sublattices of the honeycomb structure.^{9,11} More generally, the parity in this continuum model cannot be preserved simultaneously with the time-reversal invariance near the edge of the system. This is closely related to the existence of time-reversal symmetric, propagating edge states¹¹ which have become a topic of vigorous graphene-related research (see, e.g., Refs. 13,14,15,16,17,18,19,20,9,21). The time-reversal symmetry requires that the edge states from the different valleys propagate in the opposite directions, forming a Kramers pair at a given energy. As a result, even in the absence of the intervalley scattering the problem does not reduce to a single valley, in the sense that the valley contributions to observables are not identical. For the low-energy states (imitating the RH and LH fermions), this implies broken Dirac fermion parity.

We intend to demonstrate several new properties of the broken-parity edge states:

- (i) nonanalytic particle-hole asymmetry of local and global densities of states,
- (ii) time-reversal invariant pseudospin polarization (which in graphene is associated with the sublattice degree of freedom), and
- (iii) asymmetric nonlinear bias-voltage dependence of the tunneling conductance.

In view of the progress in experimental control over graphene edges,²² this material is particularly suitable to test our findings. Below we discuss in more detail the connection between our results and the ongoing graphene-related research.

Our finding (i) can be tested by means of scanning tunneling spectroscopy (STS) of the density of states (DOS). In fact, some STS experiments^{14,15} have already reported a particle-hole asymmetric DOS with a peak at -20-50 meV for monoatomic zigzag graphene edges.

By contrast Li et al.²³ have observed a symmetric linear DOS in graphene bulk. In our model, the crossover from an asymmetric edge DOS to a symmetric bulk one follows naturally from the existence of the broken-parity Dirac fermion edge states. The results of experiments^{14,15} could therefore provide some evidence for the Dirac fermion parity violation. Such an interpretation is also supported by the observation that the position of the DOS peak in the experiment of Niimi et al.¹⁵ can be described very accurately by our model. This is achieved by taking into account not only the structural asymmetry but also a potential-energy difference between the sublattices⁹ that generates weakly dispersive edge states rather than the singular zero-energy band.¹¹ It was shown earlier¹⁷ that the next-nearest-neighbor hopping on the honeycomb lattice could also result in a particle-hole asymmetric edge DOS. However, this symmetry-breaking mechanism results in the DOS peak at significantly larger energies, of the order of next-nearest-neighbor hopping energy ≈ 300 meV.

Another our result **(ii)** demonstrates that broken-parity edge states carry a time-reversal-invariant pseudospin polarization. This agrees with the general perception that in graphene electronic properties and those arising from the sublattice degree of freedom (pseudospin) are interrelated. However, there is a great deal of uncertainty as to how such a relation can be studied. The specific feature of our edge problem is that it is possible to establish a one-to-one correspondence between the pseudospin polarization and the edge DOS. We suggest that the pseudospin polarization can be detected via measurements of the electric conductance in lateral tunnel contacts between zigzag-terminated graphene and a suitably chosen metallic electrode.

Our proposal is based on finding **(iii)** that the edge-state (i.e. polarization-dependent) contribution to the conductance is asymmetric with respect to the bias voltage. Therefore, it can be separated from the symmetric contribution of the bulk graphene states. In addition, the edge-state tunnel conductance turns out to be strongly nonlinear: It exhibits kink-like switching as the sign of the voltage reverses. Such a behavior could serve as a prototype for the potentially useful electronic functionality.

The outline of the paper is as follows. In Sec. II we formulate the boundary problem for the Green's function of the Dirac equation and discuss the role of the parity symmetry. In Sec. III we analyze the local DOS and pseudospin polarization, and compare our results for the local DOS with the experimental data of Niimi et al.¹⁵ Section IV describes the relation between the global edge DOS and pseudospin polarization and their tunneling spectroscopy. The last section V summarizes our results and discusses their validity as well as possible applications.

II. DIRAC FERMIONS IN 2D SEMI-SPACE: BROKEN PARITY AND EDGE STATES

Edge-state spectroscopy usually deals with isolated edges in large samples where finite-size effects are presumably irrelevant.^{14,15,22} We model this by considering a boundary problem for a Dirac fermion retarded Green's function in a 2D semi-space $-\infty < x < \infty$, $0 < y < \infty$:

$$(\varepsilon I - v\gamma^5 \Sigma \mathbf{p}) G_\varepsilon(\mathbf{r}, \mathbf{r}') = \delta(\mathbf{r} - \mathbf{r}'), \quad (1)$$

$$G_\varepsilon = \left(\frac{I + \gamma^5}{2} \Sigma \mathbf{n}_+ + \frac{I - \gamma^5}{2} \Sigma \mathbf{n}_- \right) G_\varepsilon|_{y=0}, \quad \mathbf{n}_\pm^2 = 1, \quad (2)$$

with $G|_{y \rightarrow \infty}$ being finite. In Eq. (1) $\mathbf{p} = -i\hbar(\partial_x, \partial_y, 0)$, ε and v are the 2D momentum operator, energy and velocity near a Fermi point. In view of the further analysis of the parity symmetry, equations (1) and (2) are both expressed in terms of the chirality, γ^5 and effective spin, Σ through the Dirac matrices:⁷

$$\begin{aligned} \gamma^5 &= i\gamma^0\gamma^1\gamma^2\gamma^3 = \tau^3 \otimes \sigma^0, & \Sigma &= \gamma^5\gamma^0\gamma = \tau^0 \otimes \sigma, \\ \gamma^0 &= -\tau^1 \otimes \sigma^0, & \gamma &= i\tau^2 \otimes \sigma. \end{aligned} \quad (3)$$

We introduce the two sets of Pauli matrices, $\sigma^{1,2,3}$ and $\tau^{1,2,3}$, and the corresponding unit matrices, σ^0, τ^0 and $I = \tau^0 \otimes \sigma^0$. In graphene, $\sigma^{1,2,3}$ represent the two sublattices of the honeycomb structure, while $\tau^{1,2,3}$ act in the valley space. The eigenstates and eigenvalues ($\tau = \pm 1$) of the hermitean matrix γ^5 conventionally define the right-handed (RH, +) and left-handed (LH, -) quasiparticles⁷. In Eqs. (1) and (2) they are described by the projected Green's functions $\frac{1}{2}(I \pm \gamma^5)G_\varepsilon$.

The boundary condition, Eq. (2) ensures vanishing of the particle current across the edge^{8,9} (i.e. no Klein tunneling²⁴). It is diagonal in chirality space with the RH and LH blocks parametrized by three-dimensional unit vectors, $\mathbf{n}_\tau = \mathbf{n}_\pm$, orthogonal to the boundary normal.^{8,9} In graphene, where $\tau = \pm 1$ label the valleys, the case of the zigzag edge corresponds to⁹

$$\mathbf{n}_+ = -\mathbf{n}_- = \hat{\mathbf{z}}, \quad G_\varepsilon = \gamma^5 \Sigma^3 G_\varepsilon|_{y=0}, \quad (5)$$

where $\hat{\mathbf{z}}$ is the out-of-plane unit vector. This implies that one of the sublattice Green's functions must vanish at the edge, reflecting the structural sublattice asymmetry of the zigzag boundary.¹¹ The other nontrivial limit is

$$\mathbf{n}_+ = \mathbf{n}_- = \hat{\mathbf{x}}, \quad G_\varepsilon = \Sigma^1 G_\varepsilon|_{y=0}. \quad (6)$$

It is the infinite mass confinement of Berry and Mondragon¹⁰ ($\hat{\mathbf{x}}$ is the unit vector along the edge). As shown in Ref. 9, the intermediate case, when \mathbf{n}_\pm interpolate between (5) and (6), can be treated as a zigzag edge where the *structural* sublattice asymmetry coexists with a *potential* (energy) sublattice asymmetry that could result from electron-electron interactions within atomic distances near the edge.²⁵ This does not however exhaust the applicability of the boundary condition (2), since it

can be derived from the only requirement that the Dirac particle current is zero in the normal direction at the edge.^{8,9}

Unless restricted to the infinite mass confinement case (6), the boundary parameters are not identical, $\mathbf{n}_+ \neq \mathbf{n}_-$, which is verified below on the basis of the time-reversal (\mathcal{T}) symmetry [see, Eq. (15)]. Therefore, boundary condition (2) (and, in particular, Eq. (5)) explicitly contains the chirality, γ^5 . This violates the symmetry under the exchange of the RH and LH quasiparticles,

$$G_\varepsilon \rightarrow \gamma^0 G_\varepsilon \gamma^0, \quad (7)$$

since it reverses the sign of γ^5 (In contrast, Σ is even under such operation). On the other hand, the RH \leftrightarrow LH exchange is involved in the parity transformation,⁷

$$G_\varepsilon(\mathbf{r}, \mathbf{r}') \rightarrow \gamma^0 G_\varepsilon(-\mathbf{r}, -\mathbf{r}') \gamma^0, \quad (8)$$

and in the particle-hole conjugation,

$$G_\varepsilon(\mathbf{r}, \mathbf{r}') \rightarrow -\gamma^0 G_{-\varepsilon}(\mathbf{r}, \mathbf{r}') \gamma^0, \quad (9)$$

both leaving the Dirac equation (1) invariant. Therefore, if boundary condition (2) deviates from the infinite mass confinement (6), our boundary problem exhibits no parity invariance and, in view of Eq. (9), no particle-hole symmetry. The symmetry breaking persists in the limit of the zigzag edge, Eq. (5). We therefore conclude that the parity breaking is due to the structural sublattice asymmetry of the zigzag-type lattice termination.¹¹ For practical calculations, we need to take into account deviations of \mathbf{n}_\pm from $\hat{\mathbf{z}}$ (e.g. due to potential-energy sublattice asymmetry⁹), because it eliminates the Green's function singularity at $\varepsilon = 0$ characteristic to dispersionless zero-energy edge states.

The connection between the parity breaking and the existence of the edge states can be established by explicit calculation of the Green's function from Eqs. (1) and (2). The calculation details are given elsewhere.²⁰ Here we present the final result:

$$G_\varepsilon(\mathbf{r}, \mathbf{r}') = \sum_{\tau=\pm 1, k} \left(\frac{I + \tau \gamma^5}{2} \right) \left(I + \frac{\tau v}{\varepsilon} \Sigma \mathbf{p} \right) \times \left(G_{\varepsilon\tau k}^{(0)}(y, y') I + G_{\varepsilon\tau k}^{(3)}(y, y') \Sigma^3 \right) \frac{e^{ik(x-x')}}{L}, \quad (10)$$

$$G_{\varepsilon\tau k}^{(0)}(y, y') = \frac{\varepsilon}{2\hbar^2 v^2 q} \left(e^{-q(y+y')} - e^{-q|y-y'|} \right) + \frac{q + kn_{z\tau}}{2(\varepsilon - \hbar v \tau k n_{x\tau})} e^{-q(y+y')}, \quad (11)$$

$$G_{\varepsilon\tau k}^{(3)}(y, y') = \frac{k + qn_{z\tau} - \tau \varepsilon n_{x\tau} / \hbar v}{2(\varepsilon - \hbar v \tau k n_{x\tau})} e^{-q(y+y')}, \quad (12)$$

where $q = \sqrt{k^2 - \varepsilon^2 / \hbar^2 v^2}$ and k is the wave number. In Eqs. (11) and (12) the edge states are described by the

terms with the pole at $\varepsilon = \hbar v \tau k n_{x\tau}$. Let us examine, for instance, Eq. (12) near the pole:

$$G_{\varepsilon\tau k}^{(3)}(y, y') \approx -\frac{n_{z\tau} \Theta(kn_{z\tau})}{\varepsilon - \hbar v \tau k n_{x\tau}} \partial_y e^{-|kn_{z\tau}(y+y')}. \quad (13)$$

Clearly, the pole exists only if the unit step function $\Theta(kn_{z\tau})$ is nonzero, which determines the spectrum as

$$\varepsilon_{\tau k} = \hbar v \tau k n_{x\tau}, \quad kn_{z\tau} > 0. \quad (14)$$

These equations are not yet restricted by the \mathcal{T} symmetry. The \mathcal{T} -symmetric spectrum follows from the condition that both equations (14) are invariant under the simultaneous reversal of the chirality and wave-vector, $\tau, k \rightarrow -\tau, -k$. This imposes the following restrictions on \mathbf{n}_τ :

$$n_{x\tau} = n_x, \quad n_{z\tau} = \tau n_z, \quad \mathbf{n} = (n_x, 0, n_z), \quad \mathbf{n}^2 = 1, \quad (15)$$

leaving a single free boundary parameter - the direction of the unit vector \mathbf{n} . The edge-state spectrum is now manifestly Kramers degenerate and particle-hole asymmetric:⁹

$$\varepsilon_{\tau k} = \hbar v \tau k n_x, \quad \tau k n_z > 0. \quad (16)$$

The role of the parity breaking is quite apparent from the behavior of the edge-state Green's function (13): it vanishes identically for the infinite mass confinement ($n_z = 0$) which preserves the parity symmetry (see, also Eq. (6)).

The knowledge of the spectrum (16) is not sufficient to interpret the STS measurements,^{14,15} as they provide information on the local DOS rather than dispersion $\varepsilon_{\tau k}$. In the next section we use the full Green's function (10) to calculate the local DOS of the system. We will see that in addition to the exponentially localized states (13) there is another type of edge states decaying algebraically as a consequence of the lack of the energy gap in the 2D bulk. This distinguishes our system from, e.g., topological insulators where bulk excitations are fully gapped.^{4,5,26}

III. LOCAL DOS AND PSEUDOSPIN POLARIZATION

A. Particle-hole symmetry and the role of parity

The spectral and pseudospin properties of the system are interrelated. Let us define the local DOS

$$\nu_\pm(\varepsilon, \mathbf{r}) = -\frac{1}{2\pi} \text{ImTr} (I \pm \gamma^5) G_\varepsilon(\mathbf{r}, \mathbf{r}), \quad (17)$$

and local pseudospin polarizations

$$p_\pm(\varepsilon, \mathbf{r}) = -\frac{1}{2\pi} \text{ImTr} (I \pm \gamma^5) \Sigma^3 G_\varepsilon(\mathbf{r}, \mathbf{r}) \quad (18)$$

in terms of the RH and LH projections of the Green's function, G_ε . Tunneling spectra are determined by the total local DOS related to $G^{(0)}$ in Eq. (11):

$$\nu(\varepsilon, \mathbf{r}) = \nu_+ + \nu_- = -\frac{2}{\pi L} \sum_{\tau=\pm 1, k} \text{Im} G_{\varepsilon\tau k}^{(0)}(y, y). \quad (19)$$

Likewise, $p_+ + p_- = -\frac{1}{\pi} \text{ImTr} \Sigma^3 G_\varepsilon$ is the net pseudospin polarization. It vanishes by \mathcal{T} symmetry, since Eqs. (15) yield $p_- = -p_+$. As a \mathcal{T} -invariant characteristic of the pseudospin properties, we use the chiral pseudospin polarization (CPP) related to $G^{(3)}$ in Eq. (12):

$$\begin{aligned} p(\varepsilon, \mathbf{r}) &= p_+ - p_- = -\frac{1}{\pi} \text{ImTr} \gamma^5 \Sigma^3 G_\varepsilon(\mathbf{r}, \mathbf{r}) \\ &= -\frac{2}{\pi L} \sum_{\tau=\pm 1, k} \tau \text{Im} G_{\varepsilon\tau k}^{(3)}(y, y). \end{aligned} \quad (20)$$

Integrating over k in Eqs. (19) and (20), we obtain

$$\begin{aligned} \nu(\varepsilon, y) &= \frac{2|\varepsilon|}{\pi \hbar^2 v^2} - \sum_{\tau=\pm 1} \frac{\Theta(\varepsilon \tau n_x \tau n_z \tau)}{h v |n_x \tau|} \partial_y e^{-\frac{2y}{\hbar v} |\varepsilon \frac{n_z \tau}{n_x \tau}|} \\ &- \frac{|\varepsilon|}{\pi^2 \hbar^2 v^2} \sum_{\tau=\pm 1} \int_0^{\frac{\pi}{2}} d\gamma \times \\ &\times \frac{n_{z\tau}^2 \cos\left(\frac{2\varepsilon y}{\hbar v} \sin \gamma\right) + \tau n_x \tau n_z \tau \sin \gamma \sin\left(\frac{2\varepsilon y}{\hbar v} \sin \gamma\right)}{n_{z\tau}^2 + \tan^2 \gamma}, \end{aligned} \quad (21)$$

$$\begin{aligned} p(\varepsilon, y) &= - \sum_{\tau=\pm 1} \frac{\tau n_{z\tau} \Theta(\varepsilon \tau n_x \tau n_z \tau)}{h v |n_x \tau|} \partial_y e^{-\frac{2y}{\hbar v} |\varepsilon \frac{n_z \tau}{n_x \tau}|} \\ &+ \frac{|\varepsilon|}{\pi^2 \hbar^2 v^2} \sum_{\tau=\pm 1} \int_0^{\frac{\pi}{2}} d\gamma \tan^2 \gamma \times \\ &\frac{\tau n_{z\tau} \cos\left(\frac{2\varepsilon y}{\hbar v} \sin \gamma\right) + n_x \tau \sin \gamma \sin\left(\frac{2\varepsilon y}{\hbar v} \sin \gamma\right)}{n_{z\tau}^2 + \tan^2 \gamma}. \end{aligned} \quad (22)$$

It is now easy to see that the particle-hole symmetry is controlled by the parity. In the broken-parity state with $\mathbf{n}_+ \neq \mathbf{n}_-$ given by Eqs. (15), the summation over chiralities $\tau = \pm 1$ in Eq. (21) yields an asymmetric DOS as a function of energy, ε :

$$\begin{aligned} \nu(\varepsilon, y) &= \frac{2|\varepsilon|}{\pi \hbar^2 v^2} - \frac{2\Theta(\varepsilon n_x n_z)}{h v |n_x|} \partial_y e^{-\frac{2y}{\hbar v} |\varepsilon \frac{n_z}{n_x}|} \\ &- \frac{2|\varepsilon|}{\pi^2 \hbar^2 v^2} \int_0^{\frac{\pi}{2}} d\gamma \times \\ &\times \frac{n_z^2 \cos\left(\frac{2\varepsilon y}{\hbar v} \sin \gamma\right) + n_x n_z \sin \gamma \sin\left(\frac{2\varepsilon y}{\hbar v} \sin \gamma\right)}{n_z^2 + \tan^2 \gamma}, \end{aligned} \quad (23)$$

The same is true for the CPP (22):

$$\begin{aligned} p(\varepsilon, y) &= -\frac{2n_z \Theta(\varepsilon n_x n_z)}{h v |n_x|} \partial_y e^{-\frac{2y}{\hbar v} |\varepsilon \frac{n_z}{n_x}|} \\ &+ \frac{2|\varepsilon|}{\pi^2 \hbar^2 v^2} \int_0^{\frac{\pi}{2}} d\gamma \tan^2 \gamma \times \\ &\frac{n_z \cos\left(\frac{2\varepsilon y}{\hbar v} \sin \gamma\right) + n_x \sin \gamma \sin\left(\frac{2\varepsilon y}{\hbar v} \sin \gamma\right)}{n_z^2 + \tan^2 \gamma}, \end{aligned} \quad (24)$$

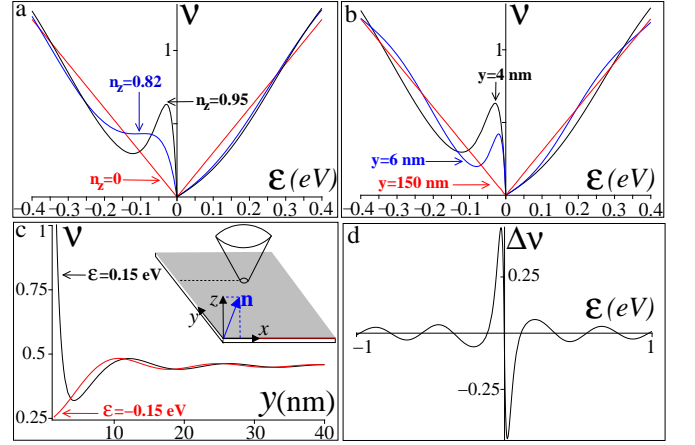


FIG. 1: (Color online) Local density of states in units of $3/4\pi \text{ eV}^{-1} \text{ nm}^{-2}$: (a) vs. energy for different n_z at $y = 4 \text{ nm}$; (b) vs. energy at different positions for $n_z = 0.95$; (c) vs. position for opposite-sign energies and $n_z = 0.95$. Inset: local STS geometry and orientation of the unit vector \mathbf{n} [Eq. (15)] determining the boundary condition (2). (d) Asymmetric local DOS $\Delta\nu \equiv \nu(\varepsilon) - \nu(-\varepsilon)$ vs. energy at $y = 5 \text{ nm}$ for $n_z = 0.95$. The data are for $v = 10^6 \text{ ms}^{-1}$ and $n_x < 0$.

For comparison, if the parity is preserved for $\mathbf{n}_+ = \mathbf{n}_-$, the DOS (21) appears to be an even function of energy:

$$\begin{aligned} \nu(\varepsilon, y) &= \frac{2|\varepsilon|}{\pi \hbar^2 v^2} - \frac{1}{h v |n_x|} \partial_y e^{-\frac{2y}{\hbar v} |\varepsilon \frac{n_z}{n_x}|} \\ &- \frac{2|\varepsilon| n_z^2}{\pi^2 \hbar^2 v^2} \int_0^{\frac{\pi}{2}} d\gamma \frac{\cos\left(\frac{2\varepsilon y}{\hbar v} \sin \gamma\right)}{n_z^2 + \tan^2 \gamma}, \end{aligned} \quad (25)$$

However, the requirements for the parity symmetry, $\mathbf{n}_+ = \mathbf{n}_-$, are incompatible with conditions (15) for the \mathcal{T} symmetry. The only exception is the infinite mass confinement limit $n_z \rightarrow 0$. In literature,^{11,21,25,27} \mathcal{T} -symmetry breaking on zigzag graphene edges has been discussed in connection with their possible intrinsic magnetism. It is still unclear whether the \mathcal{T} -symmetry breaking in the boundary condition, Eq. (2) has anything to do with the edge magnetism. We will therefore limit our analysis to the \mathcal{T} -symmetric case (15).

B. Energy and position dependence of the local DOS: Analysis

In Fig. 1 we plot the local DOS (23) as a function of energy ε (in eV) and position y (in nm) for the Fermi velocity $v = 10^6 \text{ ms}^{-1}$. These units and parameters are typical for STS in graphene. Panel (a) shows an asymmetric peak, due to the edge states, emerging on top of the linear DOS as the boundary condition varies from the Berry-Mondragon type ($n_z = 0$) to the zigzag type ($|n_z| \rightarrow 1$). In the latter case, the DOS (23) still fails to

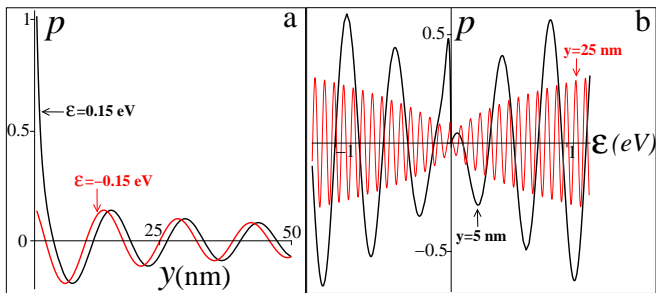


FIG. 2: (Color online) Chiral pseudospin polarization **(a)** vs. position and **(b)** vs. energy for $n_z = 0.95$ and $n_x < 0$.

recover the particle-hole symmetry because of the broken parity [see, Eq. (5)], which is formally described by the singular energy-dependent factor $\Theta(\varepsilon n_x n_z)$. The crossover between the Berry-Mondragon and zigzag cases can in principle be induced by a staggered mean-field sublattice potential whose strength is parametrized by the angle between \mathbf{n} and $\hat{\mathbf{z}}$.⁹

For $|n_z| \rightarrow 1$ the edge modes are much slower than the bulk ones, and have a small characteristic energy, $\approx \hbar v/2y \times |n_x/n_z|$. This can explain the observed DOS asymmetry on the scales of 20–50 meV¹⁵. For $n_z = 0.95$, the peak position, $\varepsilon \approx 25$ meV, and its overall behavior [panel (b)] agree very well with the observations (see, e.g., Fig. 5 in Ref. 15). As we neglect possible level broadening, the peak looks somewhat higher and narrower than in the experiment. Also, in agreement with the findings of Li et al.²³, $\nu(\varepsilon)$ approaches the symmetric Dirac DOS away from the edge. The position dependence of the DOS [panel (c)] shows that at the edge ν reaches either a maximum or a minimum depending on the presence or absence of the exponential term in Eq. (23), which is controlled only by the sign of ε . The Dirac waves, incident from the bulk and reflected from the edge, interfere yielding an oscillatory contribution (third term) in the DOS (23), decaying as $y^{-3/2}$ on the scale of 10-20 nm. Panel (d) demonstrates similar oscillations in the energy dependence.

C. Local chiral pseudospin polarization

To conclude the analysis of the local properties, in Fig. 2 we plot the CPP given by Eq. (24). From Fig. 2(a) we see that the CPP has a purely boundary origin as it decays to zero in the bulk. Apart from the presence of the oscillations, both position and energy dependences of the local CPP differ significantly from the corresponding behaviors of the local DOS [cf. Figs. 2 and 1(c,d)]. Although not obvious in the local quantities $\nu(\varepsilon, y)$ and $p(\varepsilon, y)$, in the next section we establish a direct relation between the appropriately defined global CPP and DOS.

IV. GLOBAL EDGE DOS AND PSEUDOSPIN POLARIZATION

A. Relation between the edge DOS and pseudospin polarization

Let us define the DOS and CPP of a finite region of space, $0 \leq y \leq w$, as the following dimensionless integrals,

$$N_e(\varepsilon, w) = \hbar v \int_0^w dy \left(\nu(\varepsilon, y) - \frac{2|\varepsilon|}{\pi \hbar^2 v^2} \right), \quad (26)$$

$$P(\varepsilon, w) = \hbar v \int_0^w dy p(\varepsilon, y). \quad (27)$$

In the first equation we subtract the bulk Dirac DOS, so that $N_e(\varepsilon, w)$ contains the contribution of the edge states only. By contrast to their local counterparts, it is convenient to call $N_e(\varepsilon, w)$ and $P(\varepsilon, w)$ the global edge DOS and global CPP, respectively.

Inserting Eqs. (23) and (24) into Eqs. (26) and (27) and integrating over position y , we find

$$N_e(\varepsilon) = \frac{2\Theta(\varepsilon n_x n_z)}{|n_x|} \left[1 - e^{-\frac{2w}{\hbar v} |\varepsilon \frac{n_x}{n_z}|} \right] - \frac{2n_z \text{sgn} \varepsilon}{\pi} \quad (28)$$

$$\times \int_0^{\frac{\pi}{2}} d\gamma \left[\frac{n_z}{\sin \gamma} \frac{\sin\left(\frac{2\varepsilon w}{\hbar v} \sin \gamma\right)}{n_z^2 + \tan^2 \gamma} + n_x \frac{1 - \cos\left(\frac{2\varepsilon w}{\hbar v} \sin \gamma\right)}{n_z^2 + \tan^2 \gamma} \right],$$

$$P(\varepsilon) = \frac{2n_z \Theta(\varepsilon n_x n_z)}{|n_x|} \left[1 - e^{-\frac{2w}{\hbar v} |\varepsilon \frac{n_x}{n_z}|} \right] + \frac{2 \text{sgn} \varepsilon}{\pi} \quad (29)$$

$$\times \int_0^{\frac{\pi}{2}} d\gamma \left[\frac{n_z}{\sin \gamma} \frac{\sin\left(\frac{2\varepsilon w}{\hbar v} \sin \gamma\right)}{1 + n_z^2 \cot^2 \gamma} + n_x \frac{1 - \cos\left(\frac{2\varepsilon w}{\hbar v} \sin \gamma\right)}{1 + n_z^2 \cot^2 \gamma} \right].$$

It is instructive to discuss first the limit $w \rightarrow \infty$, when the integrals in Eqs. (28) and (29) can be evaluated analytically. In this case the integrals with the rapidly oscillating cosine function vanish, while those containing the sine function should be evaluated with care since the ratio $\sin\left(\frac{2\varepsilon w}{\hbar v} \sin \gamma\right) / \sin \gamma$ becomes singular, $\pi \text{sgn}(\varepsilon) \delta(\sin \gamma)$ as $w \rightarrow \infty$. After integrating with the delta function $\delta(\sin \gamma)$, we have

$$N_e(\varepsilon) = \frac{2\Theta(\varepsilon n_x n_z)}{|n_x|} - 1 - \frac{2n_x n_z \text{sgn} \varepsilon}{\pi} \int_0^{\frac{\pi}{2}} \frac{d\gamma}{n_z^2 + \tan^2 \gamma},$$

$$P(\varepsilon) = \frac{2n_z \Theta(\varepsilon n_x n_z)}{|n_x|} + \frac{2n_x \text{sgn} \varepsilon}{\pi} \int_0^{\frac{\pi}{2}} \frac{d\gamma}{1 + n_z^2 \cot^2 \gamma}.$$

The remaining integrals are easy to evaluate²⁸. The results are

$$N_e(\varepsilon) = \frac{1 + n_z \text{sgn}(\varepsilon n_x)}{|n_x|} - 1, \quad (30)$$

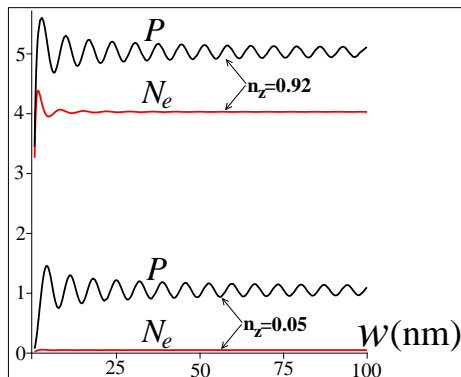


FIG. 3: (Color online) Typical behavior of the global edge DOS, N_e and chiral pseudospin polarization, P as functions of the width, w (see, Eqs. (26) – (29)).

$$P(\varepsilon) = \frac{\text{sgn}(\varepsilon n_x) + n_z}{|n_x|}, |P(\varepsilon)| = \frac{1 + n_z \text{sgn}(\varepsilon n_x)}{|n_x|}. \quad (31)$$

From Eqs. (30) and (31) we find the relation between N_e and P ,

$$N_e(\varepsilon) = |P(\varepsilon)| - 1. \quad (32)$$

Being a scalar, N_e does not depend on the sign of P which is reversed under the transformation $\mathbf{n} \rightarrow -\mathbf{n}$.

According to Eq. (32), for the zigzag graphene edge $|n_z| \rightarrow 1 (n_x \rightarrow 0)$ the absolute value of the CPP becomes equal to the edge DOS:

$$N_e(\varepsilon) \approx |P(\varepsilon)| \approx \frac{2\Theta(\varepsilon n_x n_z)}{|n_x|}. \quad (33)$$

This means that the CPP can, in principle, be detected through measurements of the global edge DOS. The latter, in turn, can be probed by tunneling, as we discuss in the next subsection. Before going to that question, we wish to point out that the correlation between P and N_e exists for finite values of w as well. Figure 3 shows the functions $N_e(w)$ [Eq. (28)] and $P(w)$ [Eq. (29)], clearly approaching the relation (32) for $w \geq 100$ nm. Note that the non-oscillatory components of P and N_e obey the relation (32) at much smaller w .

B. Tunneling spectroscopy

Our proposal for tunneling spectroscopy of the global edge DOS exploits the particle-hole asymmetric nonanalytic energy dependence of $N_e(\varepsilon)$ [Eqs. (30) and (33)]. It is essential that the particle-hole asymmetry persists in the case of zigzag-terminated graphene ($|n_z| \rightarrow 1, n_x \rightarrow 0$) because this is an experimentally accessible system.

It is known^{29,30} that a strongly energy-dependent DOS reflects in the differential electric conductance, $g(V)$ of a tunnel junction between the system of interest and a metal where the DOS is almost constant near the Fermi

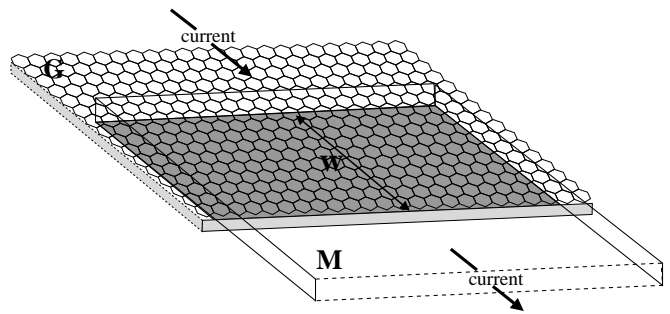


FIG. 4: (Color online) Suggested tunneling device for determining the density of the edge states in graphene. A metallic film (M) is deposited on top of a zigzag-terminated graphene sheet (G) forming a strip-like lateral contact of width, w . The device resistance is assumed to be determined by the tunnel barrier (dark gray area) so that the voltage drop V predominantly occurs between the overlapping parts of M and G.

energy. Here we consider a lateral tunnel contact between a zigzag-terminated graphene sheet and a metallic film, as shown in Fig. 4. It is assumed that the voltage drop, V , occurs predominantly across the tunnel barrier in the contact area, which determines the junction resistance. Under such condition, the conductance can be calculated using the tunneling Hamiltonian approach, which is well described in the literature (e.g. Ref. 30), with the following result:

$$g(V, T) = g_0 \int_{-\infty}^{\infty} d\varepsilon N(\varepsilon) \frac{\partial f(\varepsilon - eV, T)}{\partial (eV)}, \quad (34)$$

Here $N(\varepsilon)$ is the DOS of graphene in the contact region (dark gray area in Fig. 4), $f(\varepsilon - eV, T)$ is the Fermi-Dirac distribution of the tunneling quasiparticles at voltage V and temperature T , and the constant g_0 absorbs the energy-independent parameters of the metal and tunnel barrier. As we are interested in the low energy regime $V, T \rightarrow 0$, in Eq. (34) we can neglect inelastic tunneling processes (e.g. phonon emission).³⁰

The DOS $N(\varepsilon)$ contains the contributions of both bulk and edge states. Since the bulk DOS is a symmetric function of energy ($\propto |\varepsilon|$), it can be eliminated by taking the difference:

$$\begin{aligned} \Delta g(V, T) &= g(V, T) - g(-V, T) = \\ &= g_0 \int_{-\infty}^{\infty} d\varepsilon [N_e(-\varepsilon) - N_e(\varepsilon)] \frac{\partial f(\varepsilon - eV, T)}{\partial \varepsilon}. \end{aligned} \quad (35)$$

It contains only the particle-hole asymmetric edge DOS, $N_e(\varepsilon)$, given by Eq. (28), where w coincides with the width of the lateral tunnel contact [see, Fig. 4].

In the limit $w \rightarrow \infty$, we use Eqs. (31) and (32) to evaluate the integral in Eq. (35):

$$\Delta g(V, T) = g_0 \Delta P \tanh \frac{eV}{2k_B T}, \quad (36)$$

$$\Delta P = |P|_{\varepsilon > 0} - |P|_{\varepsilon < 0} = 2 \frac{n_z}{n_x}. \quad (37)$$

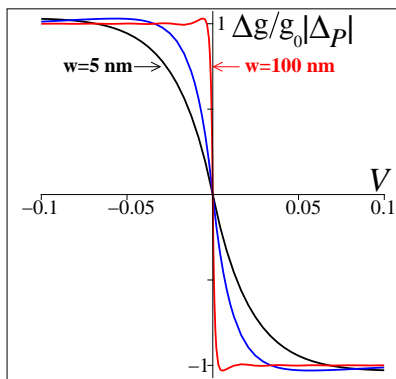


FIG. 5: (Color online) Zero-temperature conductance $\Delta g = g(V) - g(-V)$ vs. voltage (in volts) for different widths of the tunnel contact, w [see, also Fig. 4].

The conductance asymmetry $\Delta g(V, T)$ reflects the nonequilibrium quasiparticle accumulation that builds up near the graphene edge in response to the current flow between the systems. For $|eV| > 2k_B T$ the conductance $\Delta g(V, T)$ saturates at $\pm g_0 \Delta_P$, where Δ_P is the difference in the absolute values of the CPP for the positive- and negative-energy edge states. Such a nonlinear behavior can be used to detect the edge state as well as the existence of the pseudospin polarization. At zero temperature $T = 0$ the voltage dependence in Eq. (36) becomes singular ($\propto \text{sgn}(eV)$). This is specific to the $w = \infty$ limit. As shown in Fig. 5, the singularity is smeared due to finiteness of the contact width, w , so that $\Delta g(V, 0)$ saturates at voltages larger than the value $\propto w^{-1}$. The data in Fig. 5 are obtained by numerical integration of Eqs. (35) and (28) at $T \rightarrow 0$.

V. SUMMARY AND DISCUSSION

We have considered the boundary problem for 2D Dirac fermions, Eq. (1) and (2), in which the time-reversal invariance is preserved at the expense of the Dirac fermion parity. Using the Green's function solution, we have shown that the broken parity manifests itself in the density of the edge states and their pseudospin polarization, both exhibiting a nonanalytic particle-hole asymmetry. The zigzag graphene edge with its inherent structural asymmetry is an example of the realization of

the Dirac fermion parity breaking. Taking into account additionally the potential-energy sublattice asymmetry near the zigzag edge⁹, we obtain the local DOS consistent with the experimental data of Niimi et al.¹⁵ We have also established a direct correspondence between the pseudospin polarization and the density of the edge states, and suggested how to detect them in a tunneling experiment. The proposal relies on the broken particle-hole symmetry resulting in an asymmetric nonlinear contribution to the conductance, Eq. (36), in a tunnel junction between zigzag-terminated graphene and a metallic film [see, Fig. 4].

It is interesting to discuss possible implementations of the strong nonlinearity of the conductance, Eq. (36). We suggest that it could be used for detecting weak electric signals and their polarity. The operation of such a device would exploit the two different states of the tunnel junction corresponding to the conductance values at positive and negative bias voltages [see, also, Fig. 5]. Let us assume that the system is initially in one of these states. Then, under externally induced change in the bias voltage the system can switch into the state with the other (lower or higher) value of the conductance. For the zigzag graphene edge ($|n_z| \rightarrow 1, n_x \rightarrow 0$), the conductance difference, Eqs. (36) and (37), is very significant and, therefore, should be detectable. The progress in characterization of graphene edges²² may eventually lead to more understanding of how the interfaces needed to test our finding can be fabricated.

We noticed that even though the conductance, Eq. (36) vanishes for the Berry-Mondragon confinement¹⁰ ($n_z \rightarrow 0$), this case is still nontrivial, because the pseudospin polarization $P(\varepsilon)$ (32) is not zero: $P(\varepsilon) = \text{sgn}(\varepsilon n_x)$. This is confirmed by the numerical data for $n_z = 0.05$ in Fig. 3. The nonvanishing $P(\varepsilon)$ comes from the oscillatory (interference) term in Eq. (22), decaying as $y^{-1/2}$ on distances 50-100 nm [see, Fig. 2(a)]. For a given chirality (valley), the long-range polarization implies violation of the \mathcal{T} symmetry on mesoscopic scales, which may have some connection to recent studies of the level statistics in graphene quantum dots.^{31,32} Also, such long-range polarization may coexist with magnetic correlations predicted for zigzag graphene edges,^{11,21,25,27} since they are expected to decay on much shorter distances.²⁷

We thank H. Baranger, F. Guinea, M. I. Katsnelson and A. D. Mirlin for discussions. The work was supported by the Emmy-Noether Programme (DFG).

¹ We refer to the eigenstates of the Dirac chirality matrix, γ^5 , see, e.g. H. B. Nielsen and M. Ninomiya, Nucl. Phys. B **185**, 20 (1981).

² G. W. Semenoff, Phys. Rev. Lett. **53**, 2449 (1984).

³ K. S. Novoselov, A. K. Geim, S. V. Morozov, D. Jiang, M. I. Katsnelson, I. V. Grigorieva, S. V. Dubonos, and A. A. Firsov, Nature (London) **438**, 197 (2005); Y. Zhang,

Y.-W. Tan, H. L. Stormer, and P. Kim, Nature (London) **438**, 201 (2005).

⁴ M. König, S. Wiedmann, C. Brüne, A. Roth, H. Buhmann, L. W. Molenkamp, X.-L. Qi, and S.-C. Zhang, Science **318**, 766 (2007).

⁵ M. König, H. Buhmann, L. W. Molenkamp, T. Hughes, C.-X. Liu, X.-L. Qi, and S.-C. Zhang, J. Phys. Soc. Jpn.

- 77**, 031007 (2008).
- ⁶ For HgTe quantum wells, the adequacy of the Dirac fermion model has recently been discussed in M. J. Schmidt, E. G. Novik, M. Kindermann, and B. Trauzettel, arXiv: 0901.0621.
- ⁷ See, e.g., C. Itzykson and J. B. Zuber, *Quantum Field Theory* (McGraw-Hill Inc, 1985).
- ⁸ E. McCann and V. I. Fal'ko, *J. Phys. Condens. Matter* **16**, 2371 (2004).
- ⁹ A. R. Akhmerov and C. W. J. Beenakker, *Phys. Rev. B* **77**, 085423 (2008).
- ¹⁰ M. V. Berry and R. J. Mondragon, *Proc. R. Soc. Lond. A* **412**, 53 (1987).
- ¹¹ M. Fujita, K. Wakabayashi, K. Nakada, and K. Kusakabe, *J. Phys. Soc. Jpn.* **65**, 1920 (1996).
- ¹² Although this leaves out, e.g., armchair-type edges, the treatment is general enough to elucidate the origin of the parity violation.
- ¹³ K. Wakabayashi and M. Sigrist, *Phys. Rev. Lett.* **84**, 3390 (2000).
- ¹⁴ Y. Kobayashi, K. I. Fukui, T. Enoki, K. Kusakabe, and Y. Kaburagi, *Phys. Rev. B* **71**, 193406 (2005).
- ¹⁵ Y. Niimi, T. Matsui, H. Kambara, K. Tagami, M. Tsukada, and H. Fukuyama, *Phys. Rev. B* **73**, 085421 (2006).
- ¹⁶ N. M. R. Peres, F. Guinea, and A. H. Castro Neto, *Phys. Rev. B* **73**, 125411 (2006).
- ¹⁷ K. Sasaki, S. Murakami, and R. Saito, *Appl. Phys. Lett.* **88**, 113110 (2006).
- ¹⁸ L. Brey and H. A. Fertig, *Phys. Rev. B* **73**, 235411 (2006); *Phys. Rev. B* **73**, 195408 (2006).
- ¹⁹ A. Rycerz, J. Tworzydło, and C. W. J. Beenakker, *Nature Phys.* **3**, 172 (2007).
- ²⁰ G. Tkachov, *Phys. Rev. B* **76**, 235409 (2007); *Phys. Rev. B* **79**, 045429 (2009).
- ²¹ M. Wimmer, I. Adagideli, S. Berber, D. Tomanek, and K. Richter, *Phys. Rev. Lett.* **100**, 177207 (2008).
- ²² C. Ö. Girit, J. C. Meyer, R. Erni, M. D. Rossell, C. Kisielowski, L. Yang, C.-H. Park, M. F. Crommie, M. L. Cohen, S. G. Louie, and A. Zettl, *Science* **323**, 1705 (2009).
- ²³ G. Li, A. Luican and E. Y. Andrei, arXiv:0803.4016.
- ²⁴ For a recent review, see, e.g. M. I. Katsnelson, K. S. Novoselov, and A. K. Geim, *Nature Phys.* **2**, 620 (2006).
- ²⁵ Y.-W. Son, M. L. Cohen, and S. G. Louie, *Phys. Rev. Lett.* **97**, 216803 (2006).
- ²⁶ C. L. Kane and E. J. Mele, *Phys. Rev. Lett.* **95**, 226801 (2005).
- ²⁷ O. V. Yazyev and M. I. Katsnelson, *Phys. Rev. Lett.* **100**, 047209 (2008).
- ²⁸ $\int_0^{\pi/2} \frac{d\gamma}{n_z^2 + \tan^2 \gamma} = \frac{1}{2} \oint \frac{dt}{(1+t^2)(n_z^2+t^2)} = \frac{\pi}{2} \frac{1}{(1+|n_z|)|n_z|}$, and $\int_0^{\pi/2} \frac{d\gamma}{1+n_z^2 \cot^2 \gamma} = \frac{1}{2} \oint \frac{t^2 dt}{(1+t^2)(n_z^2+t^2)} = \frac{\pi}{2} \frac{1}{1+|n_z|}$, where the integration contour encircles either the upper ($\text{Im } t \geq 0$) or the lower ($\text{Im } t \leq 0$) halfplanes of the complex variable t .
- ²⁹ I. Giaever, *Phys. Rev. Lett.* **5**, 147 (1960).
- ³⁰ G. D. Mahan, *Many-Particle Physics* (Plenum Press, New York, 2000).
- ³¹ L. A. Ponomarenko, F. Schedin, M. I. Katsnelson, R. Yang, E. H. Hill, K. S. Novoselov, and A. K. Geim, *Science* **320**, 356 (2008).
- ³² J. Wurm, A. Rycerz, I. Adagideli, M. Wimmer, K. Richter, and H. U. Baranger, *Phys. Rev. Lett.* **102**, 056806 (2009).